THEORETICAL AND EXPERIMENTAL RESEARCH ON THE PRESSURE VARIATION IN THE COMPRESSION CHAMBER OF THE OIL INJECTED SCREW COMPRESSOR

Valentin PETRESCU[1], Teodor STĂNESCU[2]*, Eduard VASILE[3], Robert ISAC[4], Daniel LALE[5], Cristian SLUJITORU[6]

Oil-injected screw compressors are widely used in the compressed air industry due to their ability to reduce wear and protect internal surfaces of the compressor by injecting oil into the compression chamber. This study explores the impact of oil injection on pressure within the compression chamber of screw compressors. The investigation includes both theoretical and experimental research to improve compressor performance and optimize oil injection techniques.

Keywords: oil injected, screw compressor, pressures in compression chamber.

1. Introduction

Due to their high efficiency, compact size, and minimal maintenance needs, screw compressors have become widely employed in different industrial applications, such as refrigeration, air conditioning or natural gas processing applications. However, designing and optimizing screw compressors can be challenging due to their complex fluid dynamics and thermodynamics [1-3].

Compressors' efficiency is crucial as it directly impacts the cost of electricity consumed [4]. To optimize these machines, specialized literature presents advanced studies on rotor optimization [5], [6]. For example, these works analyze the clearances between rotors [7] and examine the influence of temperature on the compression [8]. By addressing these factors, we can enhance the effectiveness of compressors and improve their overall performance.

CFD analyses have become a popular tool in the field of gas compression providing accurate predictions of the phenomena occurring inside centrifugal compressors [9], centrifugal pumps [10] and screw compressors [11]. Using this

[1] PhD Stud. Engr.,Scientific Researcher, INCDT COMOTI, Romania,valentin.petrescu@comoti.ro
[2] PhD Stud. Engr.,Scientific Researcher, INCDT COMOTI, Romania, Correspondence e-mail: teodor.stanescu@comoti.ro
[3] Research Assistant, INCDT COMOTI, Romania, eduard.vasile@comoti.ro
[4] PhD Stud. Engr., Scientific Researcher, INCDT COMOTI, Romania, robert.isac@comoti.ro
[5] PhD Stud. Engr., Scientific Researcher, INCDT COMOTI, Romania, daniel.lale@comoti.ro
[6] Scientific Researcher III, INCDT COMOTI, Romania, cristian.slujitoru@comoti.ro

tool, one can better understand the functioning of compression units, which will lead to improving the aerodynamics of these machines.

As the understanding of these compression units is extremely important for their efficient optimization, this paper presents a simulation of unsteady flow through an oil-injected screw compressor, highlighting the behavior of gas inside the compression chambers [11-13]. To validate the obtained results, a comparison was made between the acquired data from CFD simulations and the empirical findings.

2. Description

Screw compressors are complex machines that require detailed study for proper design. To address this, the present article provides an analysis of the behavior of screw compressors at two different operating points using computational fluid dynamics (CFD) analysis methods.

Subsequently, in order to validate the simulation, an experiment was conducted on a screw compressor, measuring the pressure in the compression chamber before its opening. The measurement point was located 140 mm from the oil injection point and 103 mm from the discharge plane.

The objective of the experiment was to study the variation of air pressure during compressor operation and investigate phenomena such as over compression and under compression. Over compression refers to excessive air compression, which can lead to component damage and higher power consumption. On the other hand, under compression refers to insufficient air compression, resulting in reduced performance.

By comparing the experimental data with the results obtained from the CFD simulation, the mathematical model is validated, and its parameters can be adjusted, if necessary, to improve the accuracy of the simulation. Furthermore, this validation can be used to confirm that the CFD simulation is capable of modeling the behavior of the screw compressor under different operating conditions and can be used to make precise predictions and understand the phenomena occurring inside the machine.

3. Details of the CFD Analysis and Test Rig Presentation

The simulation of an oil-injected screw compressor is computationally and numerically highly complex due to its multiphase nature, requiring the description of interactions between air and oil, as well as the oil distribution on the rotating surfaces.

For this research, a 5/6 lobed oil-injected compressor was used, operating at speeds ranging from 500 to 1500 rotations per minute. The driving rotor has a diameter of 256.692 mm, while the driven rotor has a diameter of 202.796 mm.

The rotor length is 413 mm, with a wrap angle of 300 degrees. The clearances between rotors vary from 1 micron to 30 microns. The discharge port was designed for a volume index (V_i) of 3.5. Fig. 1 shows an image of the compressor, while Fig. 2 present a cross-section of the compressor, illustrating its main components.

Fig. 1. Screw compressor

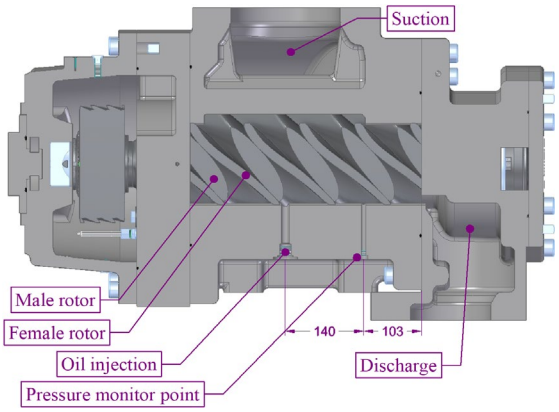

Fig. 2. Cross-section through the compressor

The 3D model served as a basis for defining the computational domain of the stator part of the screw compressor. It consists of three distinct subdomains the suction subdomain, the oil inlet subdomain and the discharge subdomain. Boolean functions were used to create the corresponding walls to delineate these subdomains. Fig. 3 illustrates the three obtained subdomains using the DesignModeler software by Ansys.

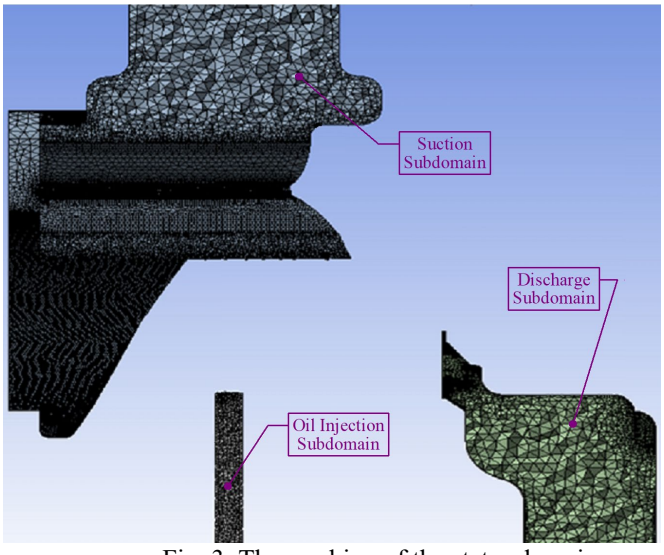

Fig. 3. The meshing of the stator domain

The number of cells that compose the computational grid is important for the results obtained in numerical simulation. A fine grid with more cells provides a more accurate simulation but can be more computationally expensive in terms of time and resources.

For simulating a screw compressor, the computational grid needs to cover the entire geometry of the compressor, including the suction and discharge regions. For this simulation, a computational grid with a total of 4,690,350 elements and 2,944,583 nodes was used. This grid (Fig. 4) was constructed using the finite volume method and adapted to cover the entire geometry of the screw compressor, including the air inlets and outlets. The large number of elements and nodes was necessary to achieve an accurate simulation of the fluid behavior in the screw compressor.

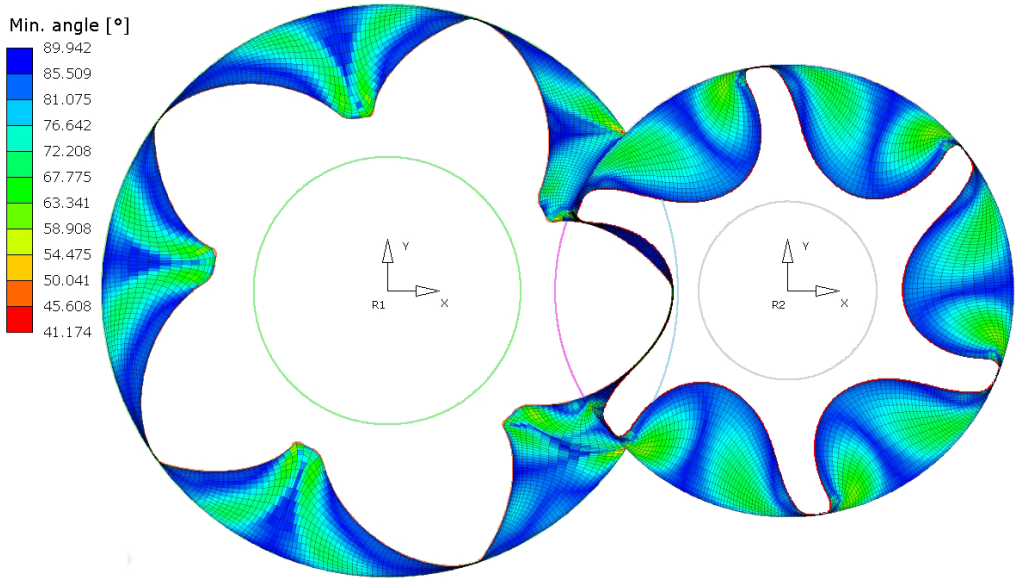

Fig. 4. Minimum angle quality between two adjacent sides of a 2D meshing element for the rotors domains

One of the main objectives of this work is to demonstrate the effectiveness of CFD simulation in the design of screw compressors. In order to achieve this objective, two case studies were conducted, in which CFD simulation was used to optimize the design of the screw compressor for a specific application. The results obtained from these case studies were analyzed to evaluate the impact of CFD simulation on the performance and efficiency of the compressor, as well as to study the variation of the air-oil mixture pressure before and during the compression process.

To achieve an accurate simulation of an oil-injected screw compressor, it is necessary to specify appropriate boundary conditions.

The initial conditions and boundary conditions used were as follows:

- Initial speed of the main rotor: 3350 rpm;
- Absolute air suction pressure: 1 bar;
- Absolute oil injection pressure: 2.5 bar;
- Absolute air discharge pressure: 7 and 9 bar;
- Initial temperature of the air: 20 °C;
- Oil injection temperature: 50 °C.

The computational grid is a graphical representation of the rotor domain division of the compressor into a set of three-dimensional cells. It is used in the simulation and modeling process to solve equations and evaluate the behavior of fluids inside the compressor.

The grid consists of a network of three-dimensional points or nodes that define the boundaries of the cells. These cells form a discretized structure of the rotor domain of the compressor, allowing for a detailed analysis of fluid flow and pressure inside it.

By using the 3D computational grid (Fig. 5), an accurate representation of the distribution of pressure, velocity, and other fluid properties in each cell of the rotor domain of the compressor can be obtained. This representation allows for a more detailed evaluation of the compressor's performance and fluid-domain interactions.

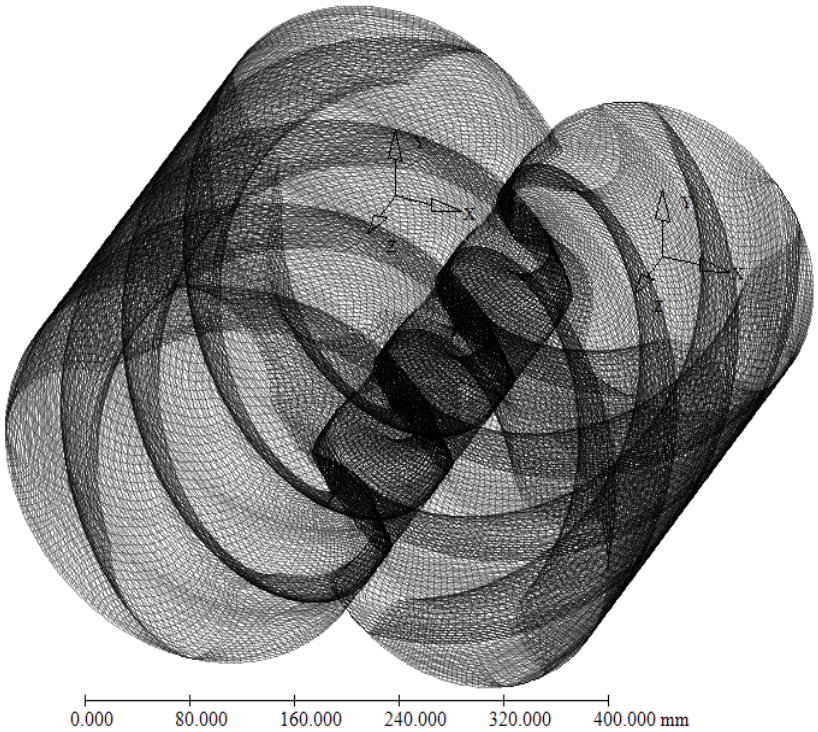

Fig. 5. The computational grid of the rotor domain

The test rig (Fig. 6) for screw compressors is equipped with a 550 kW electric motor and a speed multiplier with a transmission ratio of $i = 3.06$, which increases the rotational speed of the compressor to simulate real operating conditions. The test rig also features a magnetic speed transducer and a torque transducer that measure the operating parameters of the compressor. The screw compressor itself is present and includes oil injection on the seals, front and rear bearings, oil injection between the rotors, as well as the suction and discharge zones of the compressed air. All of these components allow for the measurement and analysis of the compressor's performance and efficiency.

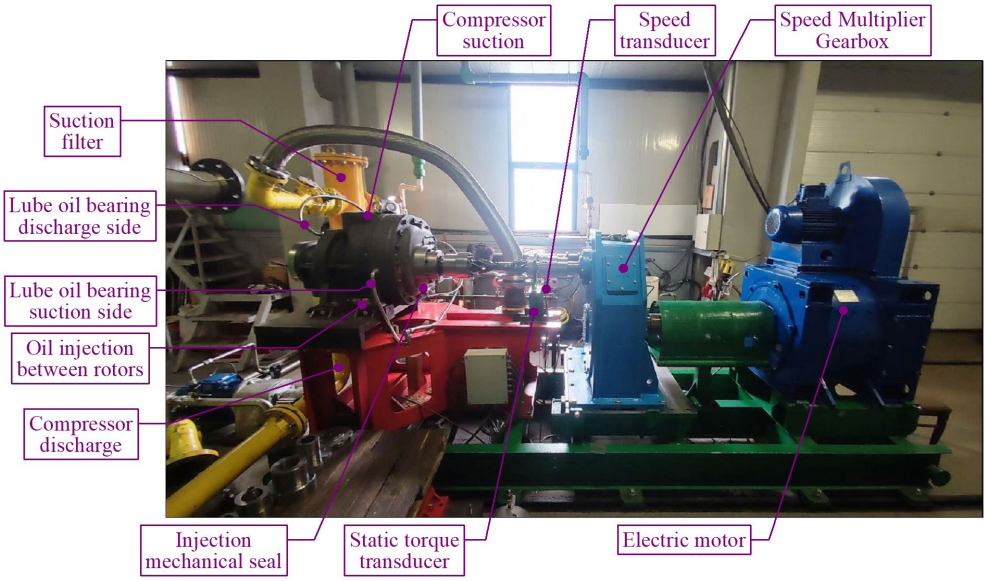

Fig. 6. The test rig of the screw compressor

To measure the pressure at the point shown in Fig. 2, the PCB Piezotronics ETM-HT-375 pressure transducer (Fig. 7) was used.

Fig. 7. The pressure transducer

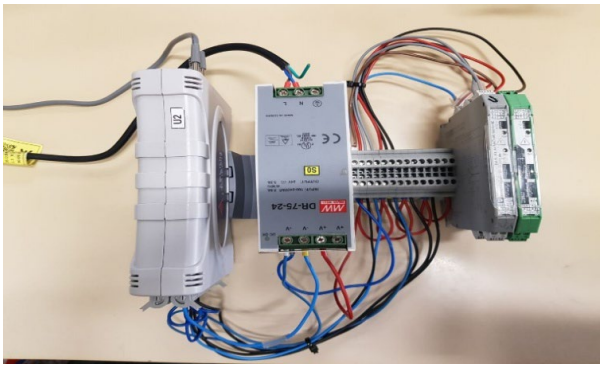

Fig. 8. The data acquisition system

This pressure sensor has a measurement range from 0 to 35 bar and can operate in environments with temperatures up to 175 °C. It has a high accuracy of ±0.5 % of the full scale, a resolution of 0.1 % of the full scale, and a sampling rate of 3 kHz.

The sensor is built with a piezoelectric element that converts pressure into an electrical signal. This electrical signal is then amplified and transmitted to a recording or control system.

The data acquisition system (Fig. 8) is represented by a portable, compact-sized system, with the following hardware components:

- An Adlink-1903 module (used for data acquisition);
- A 24V power supply;
- An input signal adapter module.

Since the Adlink-1903 module only accepts current input signals, and the transducer provides an output signal in voltage (0-5 V) at a maximum frequency of 3 kHz, a signal adaptation module has been introduced. This module converts the voltage range of the transducer (0-5 V) into a 4-20 mA signal compatible with our acquisition device. For a better understanding of the process, the pressure data from the transducer will be displayed on a real-time graph, allowing us to observe the time evolution of the signal and monitor if the pressure value remains constant.

4. Results and Discussions

The graphs (Figs. 9 and 10) represent the pressure in the last chamber over a 360-degree rotation. The x-axis represents the rotation angle in degrees, ranging from 0 to 360. The y-axis represents the pressure value.

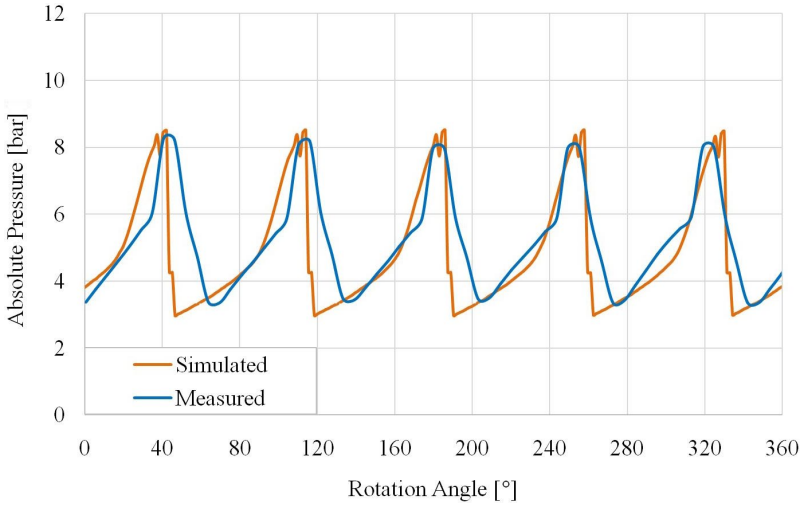

Fig. 9. Pressure variation in the last chamber at 7 bar

The orange line represents the simulated pressure in the last chamber. It is generated using a simulation model, and it consists of 240 data points evenly distributed over the 360-degree rotation. The orange line shows the simulated pressure values at each corresponding rotation angle.

The blue line represents the measured pressure in the last chamber. These pressure values have been directly measured during the rotation. The blue line consists of 63 data points, also evenly distributed over the 360-degree rotation. The blue line shows the actual measured pressure values at each corresponding rotation angle.

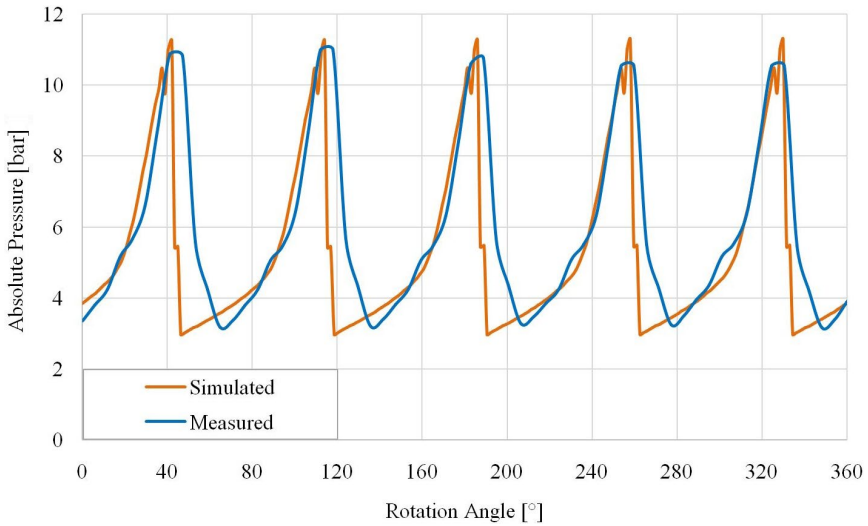

Fig. 10. Pressure variation in the last chamber at 9 bar

The differences between the measurements and simulations are small, with a similar trend of pressure increase in the compression chamber. In order to highlight the deviations between the measured values and those obtained from CFD simulations, Table 1 was created using the following formulas (1)...(4).

Table 1

Comparison between measured and simulated data

Discharge pressure [bar]	Average Pressure Value for		Deviation from the average		Min Pressure Value for		Deviation from the min value		Max Pressure Value for		Deviation from the max value	
	Measured [bar]	Simulated [bar]	[%]	[bar]	Measured [bar]	Simulated [bar]	[%]	[bar]	Measured [bar]	Simulated [bar]	[%]	[bar]
7	5.165	4.840	6.305	0.326	3.336	2.968	11.034	0.368	8.265	8.513	-3.011	-0.249
9	5.894	5.324	9.684	0.571	3.161	2.973	5.971	0.189	10.987	11.284	-2.711	-0.298

The deviation from the average, expressed as a percentage, was calculated using:

$$\varepsilon_{av} = 100 - \frac{\sum_{i=1}^{240} p_{s\,i}}{\sum_{i=1}^{63} p_{m\,i}} \cdot \frac{100 \cdot 63}{240} \tag{1}$$

where p_s represents the pressure value obtained from CFD simulations, and p_m represents the pressure value obtained experimentally.

The deviation from the average, measured in bar, was calculated using:

$$\Delta p_{av} = \frac{\sum_{i=1}^{63} p_{m\,i}}{63} - \frac{\sum_{i=1}^{240} p_{s\,i}}{240} \tag{2}$$

By employing the same formulas as previously mentioned, it is possible to calculate the deviations from the minimum or maximum values obtained during a complete 360-degree rotation. For the deviation expressed in percentage, the following formula can be used:

$$\varepsilon_{v\,min,max} = 100 - \frac{100 \cdot \min,\max(p_s)}{\min,\max(p_m)} \tag{3}$$

And for the deviation expressed in bar, it can be applied:

$$\Delta p_{min,max} = \min,\max(p_m) - \min,\max(p_s) \tag{4}$$

Additionally, for both operating points (discharge pressure of 7 and 9 bar), a deviation can be observed in the descending curves (starting from the pressure drop in the discharge chamber), indicating that during the pressure peak in the experiments, a certain linearity was observed for a few degrees (max. 6 degrees), followed by a downward trend. However, in the case of simulations, the pressure peak was recorded, and immediately after, the pressures decreased.

Furthermore, it can be observed that the slope of the curve in the case of experiments is more pronounced compared to the simulated one, resulting in a deviation up to 15 degrees at low pressure.

This suggests that the simulation effectively models the pressure behavior in the respective chamber and provides consistent results with experimental measurements. The small differences can be attributed to factors such as measurement errors, the RANS (Reynolds-averaged Navier–Stokes) mathematical model, grid refinement, et al.

5. Conclusions

The operation of the screw compressor was successfully modeled at two absolute discharge pressures, namely 7 bar and 9 bar, at a rotor speed of 3340 rpm. The simulation accurately reproduced the compressor behavior under these conditions providing results consistent with the experimentally measured values.

The pressure in the compression chamber was successfully modeled and measured during the compression and discharge process at the aforementioned pressures. The simulated and experimentally measured values showed good agreement, indicating that the utilized model is capable of effectively evaluating the pressure in the compression chamber at different stages of the compressor's operating cycle.

The obtained results indicate adequate validation of the model and support its use in assessing and optimizing the performance of screw compressors in practical applications.

R E F E R E N C E S

[1]. *P. Xavier, K. Kanthavel and R. Uma*,"Rotor Profile Design for Twin Screw Compressor", in Int. J. Sci. Eng. Res., **vol. 2**, Jan. 2011

[2]. *M. Geng, L. Wang, D. Cui, X. Li, J. Li and H. Jiang*,"Profile design of twin screw air compressor for fuel cell", in Energy Reports, **vol. 8**, Sep. 2022, pp. 21–26

[3]. *J.-G. A. Persson*,"Design parameter study to extend the capacity range of dry twin screw compressors", in IOP Conf. Ser. Mater. Sci. Eng., **vol. 1267**, Nov. 2022, p. 12009

[4]. *Ş. Şerban, S. Tomescu, I. Vladuca and S. Voicu*,"Energy improvement of an oil injected screw compressor skid", in EMERG - Energy. Environ. Effic. Resour. Glob., **vol. 7**, Jan. 2021, pp. 51–59

[5]. *J. Yang, M. Xu and Z. Lu*,"Design of Twin-Screw Compressor Rotor Tooth Profile with Meshing Clearance Based on Graphic Method and Alpha Shape Algorithm", in J. Shanghai Jiaotong Univ., **vol. 28**, Dec. 2021

[6]. *N. Stosic, I. Smith and A. Kovacevic*,"Optimization of screw compressor design", in Applied Thermal Engineering, **vol. 23**, Apr. 2023

[7]. *T. Tam, A. Kovacevic, W.J. Milligan, T. Sun, K.T.V. Grattan, M. Fabian, T. Plantegenet, B. Patel and S. Bandyopadhyay*,"Experimental Investigation Of Screw Compressor Clearance Monitoring Techniques Monitoring Techniques", in 26th International Compressor Engineering Conference at Purdue, July 2022

[8]. *A. Noskov and M. Shaposhnikova*,"Capacity regulation of refrigeration screw compressor at condensation temperature decrease", in AIP Conference Proceedings, **vol. 2285**, 2020, p. 030021

[9]. *M. Fuehne, F. Lou and N. Key*,"Experimental and Numerical Investigation of Clearance Effects in a Transonic Centrifugal Compressor", in J. Propuls. Power, **vol. 38**, Feb. 2022, pp. 1–11

[10]. *M. Rakibuzzaman, K. Kim and S.-H. Suh*,"Numerical and experimental investigation of cavitation flows in a multistage centrifugal pump", in J. Mech. Sci. Technol., **vol. 32**, Mar. 2018, pp. 1071–1078

[11]. *M. Nitulescu, C. Slujitoru, V. Petrescu, V. Silivestru, G. Fetea and S. Tomescu*,"Reducing rotors clearance - a way to increase the performance of a screw compressor", in IOP Conf. Ser. Mater. Sci. Eng., **vol. 1180**, no. 1, 2021, p. 12007

[12]. *C. Săvescu, V. Petrescu, I. Vlăducă, D. Comeagă, C. Nechifor and F. Niculescu*,"Theoretical and Experimental Analysis of a Twin-Screw Compressor as Potential Source for Vibration Energy Harvesting", in Rev. Roum. des Sci. Tech. - Série Électrotechnique Énergétique, **vol. 68**, 2023

[13]. *V. Petrescu, C. Săvescu, T. Stănescu, C. Nechifor, M. Vasile and S. Tomescu*,"Experimental analyses of twin-screw compressors' energetic efficiency depending on the volume ratio", in 11th Int. Conf. Therm. Equipment, Renew. Energy Rural Dev. (TE-RE-RD 2023), 2023